Multivariate analysis reveals activation-primed fibroblast geometric states in engineered 3D tumor microenvironments

Saradha Venkatachalapathy[a], Doorgesh Sharma Jokhun[a], and G. V. Shivashankar[a,b,c,d,*]
[a]Mechanobiology Institute and Department of Biological Sciences, National University of Singapore, 117411, Singapore; [b]FIRC Institute for Molecular Oncology, Milan 20139, Italy; [c]Department of Health Sciences and Technology, ETH Zurich, Zurich, Switzerland; [d]Paul Scherrer Institut, 5232 Villigen, Switzerland

ABSTRACT **Fibroblasts are a heterogeneous group of cells comprising subpopulations that have been found to be activated in the stromal microenvironment that regulates tumor initiation and growth. The underlying mechanisms of such selective activation of fibroblasts are not understood. We propose that the intrinsic geometric heterogeneity of fibroblasts modulates the nuclear mechanotransduction of signals from the microenvironment, resulting in their selective activation. To test this, we developed an engineered 3D fibroblast tumor coculture system and used high resolution images to quantify multiple cell geometry sensitive nuclear morphological and chromatin organizational features. These features were then mapped to activation levels as measured by the nuclear abundance of transcription cofactor, megakaryoblastic leukemia, and protein levels of its target, αSMA. Importantly, our results indicate the presence of activation-"primed" cell geometries that present higher activation levels, which are further enhanced in the presence of stimuli from cancer cells. Further, we show that by enriching the population of activation-primed cell geometric states by either increasing matrix rigidity or micropatterning primed cell shapes, fibroblast activation levels can be increased. Collectively, our results reveal important cellular geometric states that select for fibroblast activation within the heterogenous tumor microenvironment.**

Monitoring Editor
Alex Dunn
Stanford University

Received: Aug 6, 2019
Revised: Dec 24, 2019
Accepted: Jan 31, 2020

INTRODUCTION

Fibroblasts are connective tissue cells and in vivo, they are embedded in and adhered to the fibrillar extracellular matrix where they are exposed to varying local mechano-chemical signals. As a result, they occupy distinct mechanical states as seen by the variety of cell geometries they exhibit. Geometry is an intrinsic cellular property that modulates nuclear mechanics (Makhija *et al.*, 2015), the spatial organization of the genetic material (Wang *et al.*, 2017), nuclear signaling, and transcription programs (Jain *et al.*, 2013). Importantly, recent studies have demonstrated that cells in two different geometrical states have different transcriptional responses to the same stimuli (Mitra *et al.*, 2017; Damodaran *et al.*, 2018). Hence, cellular perception and response to the microenvironmental signals is dependent on their cell geometry. As a result, cell geometry modulates many important functions such as proliferation, apoptosis, cellular reprogramming, and stem cell differentiation (Chen *et al.*, 1997; McWhorter *et al.*, 2013; Uhler and Shivashankar, 2017; Roy *et al.*, 2018).

In tissues the generally quiescent fibroblasts become activated in response to microenvironmental cues comprising both physical forces (e.g., matrix rigidity, compression/tensile forces) and soluble chemical signals (e.g., cytokines, hormones) (Grinnell, 2003; Kalluri, 2016). The activation of fibroblasts is a crucial event in tissue repair and disease progression. Importantly, in the tumor microenvironment stromal fibroblasts sense stimuli released by cancer cells to become cancer-associated fibroblasts, which are important

This article was published online ahead of print in MBoC in Press (http://www.molbiolcell.org/cgi/doi/10.1091/mbc.E19-08-0420) on February 5, 2020.

The authors declare that they have no competing interests.

Author contributions: S.V., D.J., and G.V.S. designed research; S.V. and D.J. performed research; S.V., D.J., and G.V.S. analyzed data; and S.V. and G.V.S. wrote the paper.

*Address correspondence to: G.V. Shivashankar (shiva.gvs@gmail.com).

Abbreviations used: αSMA, alpha-smooth muscle actin; BSA, bovine serum albumin; CMI, cell morphology index; F-actin, filamentous actin; FWHM, full width half maxima; HC, heterochromatin; LD, linear discriminant; LD1, first linear discriminant; LDA, linear discriminant analysis; MKL, megakaryoblastic leukemia; MRTF-A, myocardin-related transcription factor; PBS, phosphate-buffered saline; PCA, principle component analysis; PDMS, polydimethylsiloxane.

regulators of tumor growth and metastasis (Kalluri, 2016; Erdogan *et al.*, 2017; Richards *et al.*, 2017). Recent studies have highlighted the existence of molecularly, morphologically, and functionally distinct fibroblast subpopulations in the normal and tumor-stromal environments (Bauer *et al.*, 2010; Kiskowski *et al.*, 2011; Öhlund *et al.*, 2014; Avery *et al.*, 2018; Philippeos *et al.*, 2018; Xie *et al.*, 2018). In addition to the studies that have used single cell transcription and protein expression profiles to explore the origins of such heterogeneity (Philippeos *et al.*, 2018; Xie *et al.*, 2018), the contribution of cellular mechanics is just beginning to be recognized (Lee *et al.*, 2014; Labriola and Darling, 2015; Herum *et al.*, 2017; Tsuboi *et al.*, 2017; Avery *et al.*, 2018; Nassiri and McCall, 2018). A quantitative description of the link between cell geometric heterogeneity and nuclear mechanotransduction in physiologically relevant 3D fibroblast tumor microenvironments has not been established.

In this paper we investigate whether the heterogeneity in cell geometry is directly coupled to the variance in fibroblast activation levels in the 3D fibroblast cancer spheroid coculture system. Using high resolution microscopy, we obtain multiple cell geometry descriptive single cell measurements of nuclear morphology and chromatin organization as well as fibroblast activation levels in the same cells. The activation level was characterized using cellular levels of alpha-smooth muscle actin (αSMA) as well as nuclear abundance of its transcription factor, megakaryoblastic leukemia (MKL) (Miralles *et al.*, 2003). Using multivariate analysis, we demonstrate that the coupling between cell geometry and nuclear abundance of MKL and αSMA is enhanced in the presence of signals released by metastatic breast cancer cells, MCF7. Further, we show that this activation can be controlled by enriching the population of activation-primed cell geometric states by either changing matrix rigidity or micropatterning specific cell shapes.

RESULTS

Fibroblast activation in engineered 3D fibroblast tumor coculture system

We embedded spheroids of the metastatic breast cancer MCF7 cells along with NIH3T3 fibroblasts in a 3D collagen matrix, thereby mimicking a tumor-stromal environment (Asghar *et al.*, 2015) (Figure 1A; see *Materials and Methods*). Within 24 h, there were physical interactions between cancer cells and fibroblasts (Figure 1B; Supplemental Figure S1A). After 72 h, we stained for αSMA (Figure 1C and Supplemental Figure S1B), a fibroblast activation marker which is also associated with increased fibroblast contractility (Hinz *et al.*, 2013). We measured the levels of αSMA within 2 μm of the fibroblast nuclear boundary and obtained the fraction of positive cells based on a threshold (Figure 1D and Supplemental Figure S1C; see *Materials and Methods*). As expected, we find a larger fraction of activated fibroblasts in the cocultured system (Stuelten, 2005). The increased contractility of these cocultured fibroblasts is evidenced by the higher shrinkage of the collagen gel (Supplemental Figure S1, D and E) (Yang *et al.*, 2015). Next, we stained for TGFβ effector transcription cofactor, MKL, and found that its nuclear abundance was also ~40% higher in cocultured fibroblasts (Figure 1E and Supplemental Figure S1, F and G). Consistently, nuclear MKL levels were positively correlated with cellular αSMA levels whereby αSMA-positive cells have higher nuclear MKL levels (Supplemental Figure S1, H and I, and Figure 1F). These results show that in the presence of cancer cells, there is an increase in the TFGβ signaling in fibroblast. Interestingly, while there is a population level increase in the nuclear MKL and cellular αSMA levels (activation markers) in the cocultured fibroblasts, there is also an increase in their variance, leading to a long-tailed distribution (Figure 1F; Supplemental Figure S1, J and K). This indicates that, in contrast to a uniform increase, only a subset of the population presents higher levels of activation. In addition to the heterogeneity in the activation levels, a variety of cellular geometric states are observed in both control and cocultured fibroblasts (Figure 1C). We hypothesized that the heterogeneity in the fibroblast activation is tuned by the fibroblast cell geometry.

Multivariate analysis for mapping cell shape to fibroblast activation levels

To test whether there is a coupling between cell geometry and fibroblast activation, we computed a cell geometry sensitive feature set for each cell and mapped it to its transcription parameters (e.g., nuclear MKL levels, αSMA levels). Calculating single cell geometric features were made difficult by the frequent overlapping and clustering of fibroblasts as shown in Figure 1B. Fibroblasts, being adherent cells, have elaborate cytoskeletal networks that connect focal adhesions to the nuclear membrane via LINC complexes which, in turn, are connected to the chromatin. This allows the extracellular forces to be directly coupled to the chromatin dynamics within the nucleus (Li *et al.*, 2015). Thereby, the morphology and the mechanical state of the nucleus and the organization of the chromatin within are directly modulated by and coupled to the geometry of the cell (Li *et al.*, 2014; Wang *et al.*, 2017). Therefore, we decided to use the nucleus and the chromatin as a sensor and descriptor of cell geometric states. HC foci are condensed chromatin present at the peri-centromere of each chromosome. Therefore, the positions of these foci are a reflection of the packing of the chromosomes within the nucleus. To characterize the nuclear mechanical heterogeneity, sets of parameters describing nuclear morphometrics, global chromatin compaction, and the organization of HC nodes were quantified (Figure 2; see *Materials and Methods*). The analytical workflow used to map cell geometric states to nuclear levels of MKL in fibroblasts embedded in a 3D collagen matrix is summarized in Figure 2. First, individual fibroblast nuclei were segmented in 3D space; this was followed by the identification of HC nodes.

To test whether our parameter set could discriminate cells of different geometries, we obtained two homogeneous populations consisting of rectangular (1800 μm^2 AR 1:5) and circular (500 μm^2) cells using micropatterned substrates (Supplemental Figure S2, A and B; Supplemental Information) (Théry, 2003). We then computed the aforementioned parameters followed by dimension reduction using principle component analysis (PCA). Cells of different geometries occupy distinct regions in the PCA biplot (Supplemental Figure S2C). We decided to use the first three principle components (~85% of variance; Supplemental Figure S2D) to represent the parameter set. The discriminative potential of this reduced parameter space was determined by maximizing interclass separation using linear discriminant analysis (LDA) (Jain *et al.*, 2000) (Supplemental Figure S2E). The classification power of LDA is tabulated in Supplemental Figure S2F (accuracy: training [94%] and validation [95.4%]). It is important to note that the parameter sets individually and combined were able to discriminate rectangular and circular cells (test accuracies > 80%; Supplemental Figure S2G).

The above results confirm that the nuclear morphology and chromatin organization are sensitive to cell geometry and therefore can be used as markers to delineate different cell geometric states in a heterogeneous cell population. Hence for each fibroblast nuclei in the 3D collagen gel, the aforementioned parameter set was computed. Its dimensionality was then reduced using PCA and the first three principle components were used to represent the cell

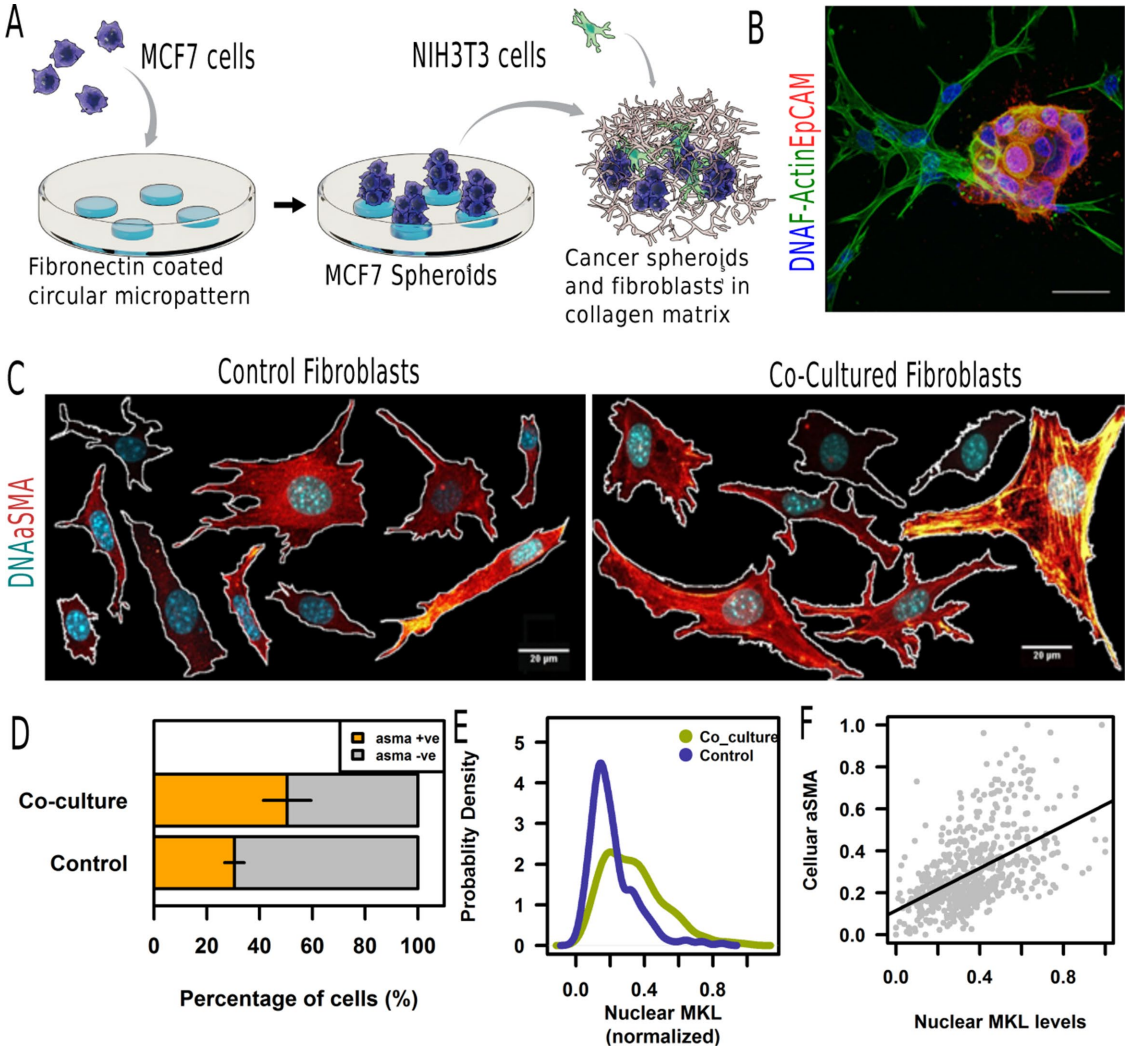

FIGURE 1: Fibroblast activation in engineered 3D fibroblast tumor coculture system. (A) Schematic representation of the engineering of a coculture system (see *Materials and Methods*). (B) Nearest point projection image depicting fibroblasts physically interacting with the MCF7 spheroid. Cells are stained for F-Actin (green) EpCAM (red), and DNA (blue). Scale bar: 20 μm. (C) Maximum intensity projections of control and cocultured fibroblasts stained for aSMA (heat colors) and DNA (cyan). Note: This is a collage of cells from different fields of view. (D) The percentage of a-SMA expressing (+ve: positive: orange) cells in the two samples visualized as a stacked barplot. The means are significantly different ($p < 2.6e\text{-}6$, Wilcox's *t* test). Segments represent the standard error of mean across three trials. (E) Probability density histogram of nuclear MKL levels in control (blue) and cocultured fibroblasts (green). The means are significantly different ($p < 1.6e\text{-}6$, Wilcox's *t* test). (F) Relationship between cellular aSMA and nuclear MKL levels. The number of cells in each sample > 800.

geometric feature space. For the same cells, the levels of MKL in the nucleus were measured. At the population level, the gradation of MKL-enriched fibroblasts was discretized by binning the MKL distribution into 10 subpopulations with an equal number of cells (deciles). LDA using the first three principle components was then used to obtain maximum separation of the subpopulations. This is then visualized in LDA biplot (Supplemental Figure S2H). The intersection ratio between the 95% confidence ellipsoids of subpopulations in the LDA space is used as a measure of the discriminatory power of the parameter set. The pairwise intersection ratios of all subpopulations (Supplemental Figure S2I) shows that the MKL-enriched nuclei have minimal overlap with the MKL-depleted nuclei. The degree of separation of nuclear MKL subpopulations by the reduced parameter space is quantified by the inverse relationship between the mean intersection ratio of ellipsoids and the number of deciles the subpopulations were apart (Supplemental Figure S2J). Of the various parameter sets, the discriminating potential of the nuclear morphological features is the highest. Since the different subpopulations of MKL nuclear levels occupy distinct regions in the LDA biplot, we conclude that cell geometry is coupled to nuclear MKL levels. In the next section, we further explore this coupling in both control and cocultured fibroblasts.

Fibroblast activation level is coupled to cell geometric states

At the population level, the cell geometric states are similar between control and cocultured fibroblasts (Figure 3A; Supplemental Figure S3A). A small fraction of the cocultured fibroblasts exhibits slightly more elongated nuclear morphologies. The nuclear abundance of MKL is tightly coupled to the cell geometry sensitive parameters in

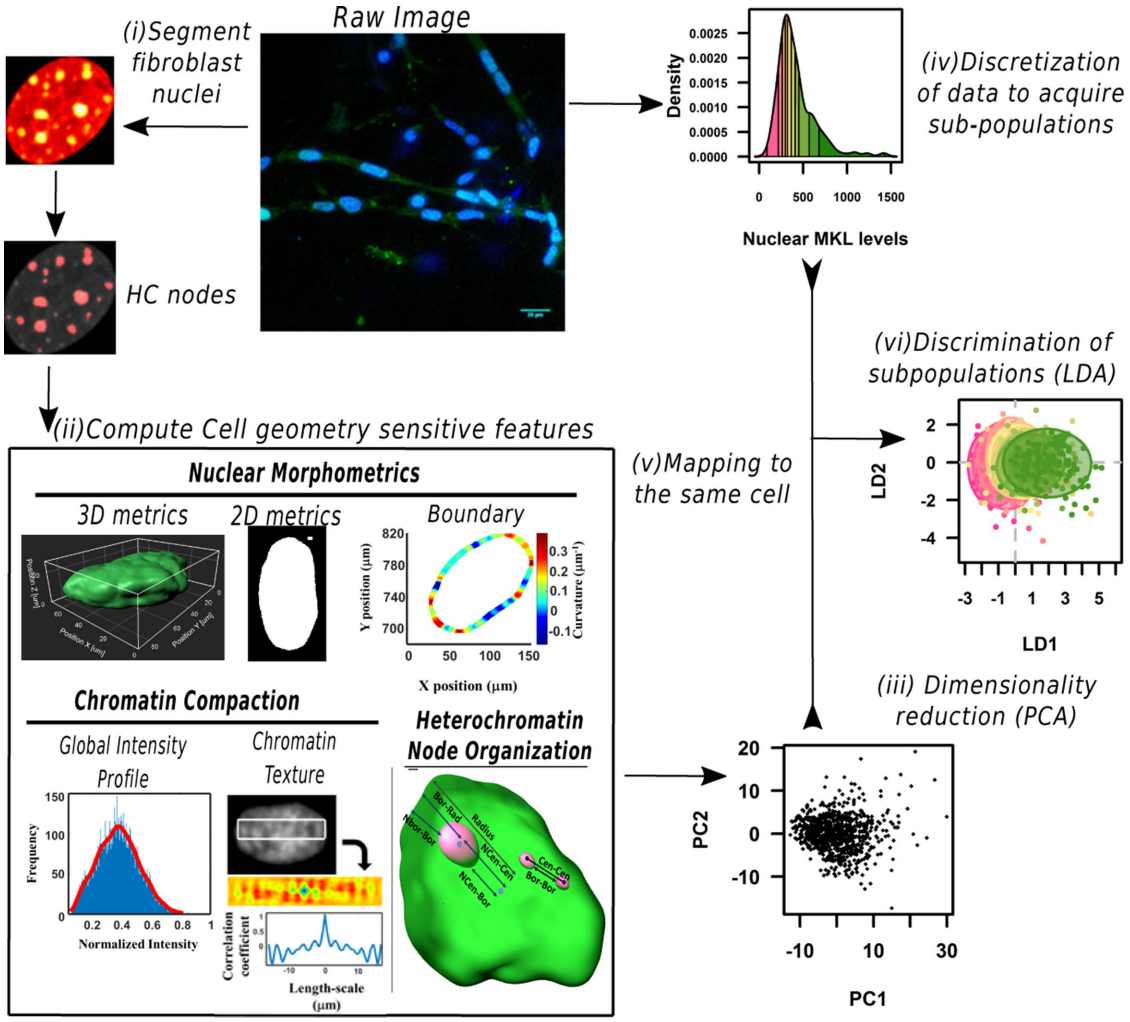

FIGURE 2: Multivariate analysis for mapping cell shape to fibroblast activation levels. (i) From the raw image, individual 3D fibroblast nuclei are identified. Next from the obtained single nucleus, HC (HC) nodes are identified. (ii) Multiple cell geometrysensitive features that describe the nuclear morphology, chromatin compaction and HC node organization are computed (n = 141) (see Supplemental Figure S2). (iii) The dimensionality of this multiparametric feature set is reduced using PCA. (iv) In parallel, the nuclear MKL levels of the identified nuclei in is measured and the probability density histogram of the nuclear MKL levels is discretized. The subpopulations of fibroblast nuclei were obtained by binning the MKL distribution into 10 subpopulations (deciles). (v) This is mapped to the same cell in the PCA space (Supplemental Figure S2). (vi) LDA using the first three principle components is used to separate the subpopulations.

both control and cocultured fibroblasts (Figure 3B; Supplemental Figure S3, B and C). We used the first linear discriminant (LD1), which we will refer as cell morphology index (CMI) to describe the cell geometric state. Nuclear MKL levels varied linearly with CMI (Figure 3C; Supplemental Figure S3D) such that the higher the CMI the greater the nuclear abundance of MKL. Importantly, the slope of this linear relationship increases by ~40% in cocultured fibroblasts when compared with control fibroblasts without much change in the CMI values (Supplemental Figure S3, A and E). Hence, cells with high CMI in control condition already have higher nuclear MKL levels which are further increased in the presence of cancer cells. In contrast, cells with low CMI have low nuclear MKL levels and this level does not change by much even in the presence of cancer cells. This suggests the presence of certain cell geometric states (CMI > 0), which are "primed" for higher activation in the presence of a stimulus. Consistently, the αSMA-positive cells had higher CMI (Figure 3D).

The top 20 parameters that show the highest correlation with CMI are shown in Figure 3E. From this map, it is evident that the MKL-enriched nuclei with higher CMI are larger in size, with a smooth boundary where the HC nodes are centrally positioned. A few representative cells with increasing CMI are depicted in Figure 3F were these differences in nuclear morphology, chromatin organization, cell geometry and fibroblast activation levels are visible. The relationships between all the parameters and CMI are summarized in Supplemental Figure S3F. Collectively, our method shows that fibroblast activation levels are coupled to cell geometric states whereby certain cell geometries are more prone to activation by cancer cells.

Since the relative distances of the fibroblasts from the cancer spheroids in each matrix as well as number and size of spheroids are variable in 3D coculture system, we next tested whether the conditioned media from the MCF7 cells can be used instead (Lewis *et al.*, 2004). The results obtained using cocultured fibroblasts were reproduced in fibroblasts exposed to conditioned media obtained from MCF7 cells for 72 h (Supplemental Figure S3, G–L). In experiments using conditioned media, the

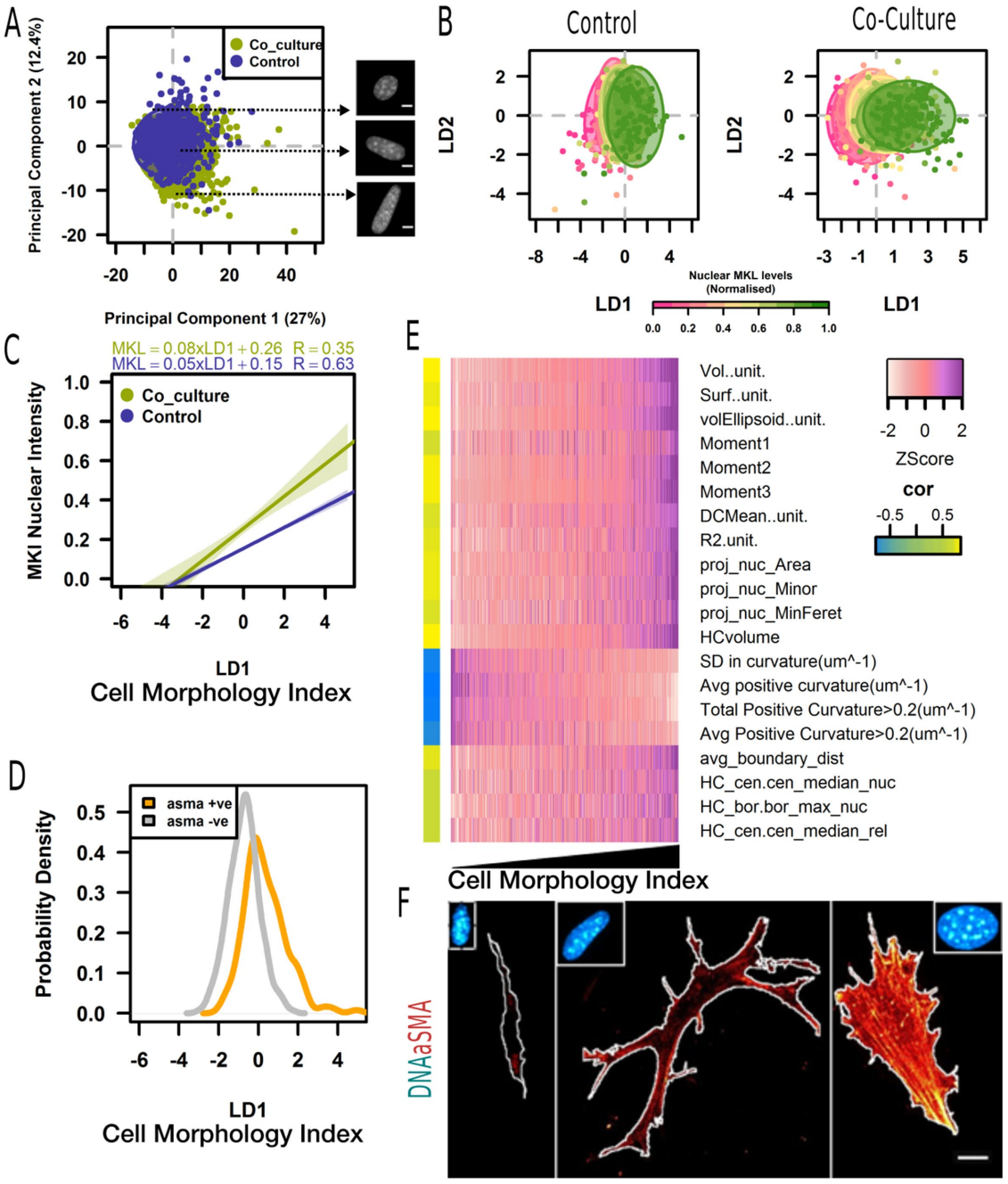

FIGURE 3: Fibroblast activation level is coupled to cell geometric states. (A) PCA biplot of the first two components obtained from multiple parameters with each circle colored based on the sample. Micrographs of nuclei are mapped to their approximate location in PCA space. Scale bar = 5 μm. (B) LDA biplot of the first two components obtained from multiple parameters with each circle colored based on the nuclear MKL subpopulation for control and cocultured fibroblast. (C) MKL nuclear intensity as a function of the LD1 or CMI in the respective samples for one representative trial. The 95% CI of prediction is visualized as line bounds. (D) Probability density histogram of CMI values for aSMA positive (orange) and negative (gray) cells from three trials. The means are significantly different ($p < 0.0001$, Wilcox's *t* test). (E) Heat map depicting relationship between the CMI and the top 20 nuclear and chromatin features. Each column corresponds to one nucleus. The row side colors depict the person correlation value (cor) between CMI and the corresponding feature. (F) Representative images of cells stained for aSMA (heat colors) and DNA (blue) with increasing LD1 values (–3.5, 0.9, and 4.1, respectively). Scale bar = 10 μm (total number of fibroblasts from three trials: cocultured, 1241; and control, 843).

correlation between nuclear MKL levels and cell geometric states is further enhanced, thereby reinforcing the importance of this geometric coupling. Henceforth, we used conditioned media to perform our experiments.

Modulating fibroblast activation by tuning the distribution cellular geometric states

Since fibroblast activation levels are correlated to cell geometric states (as described by CMI), we hypothesized that tuning the

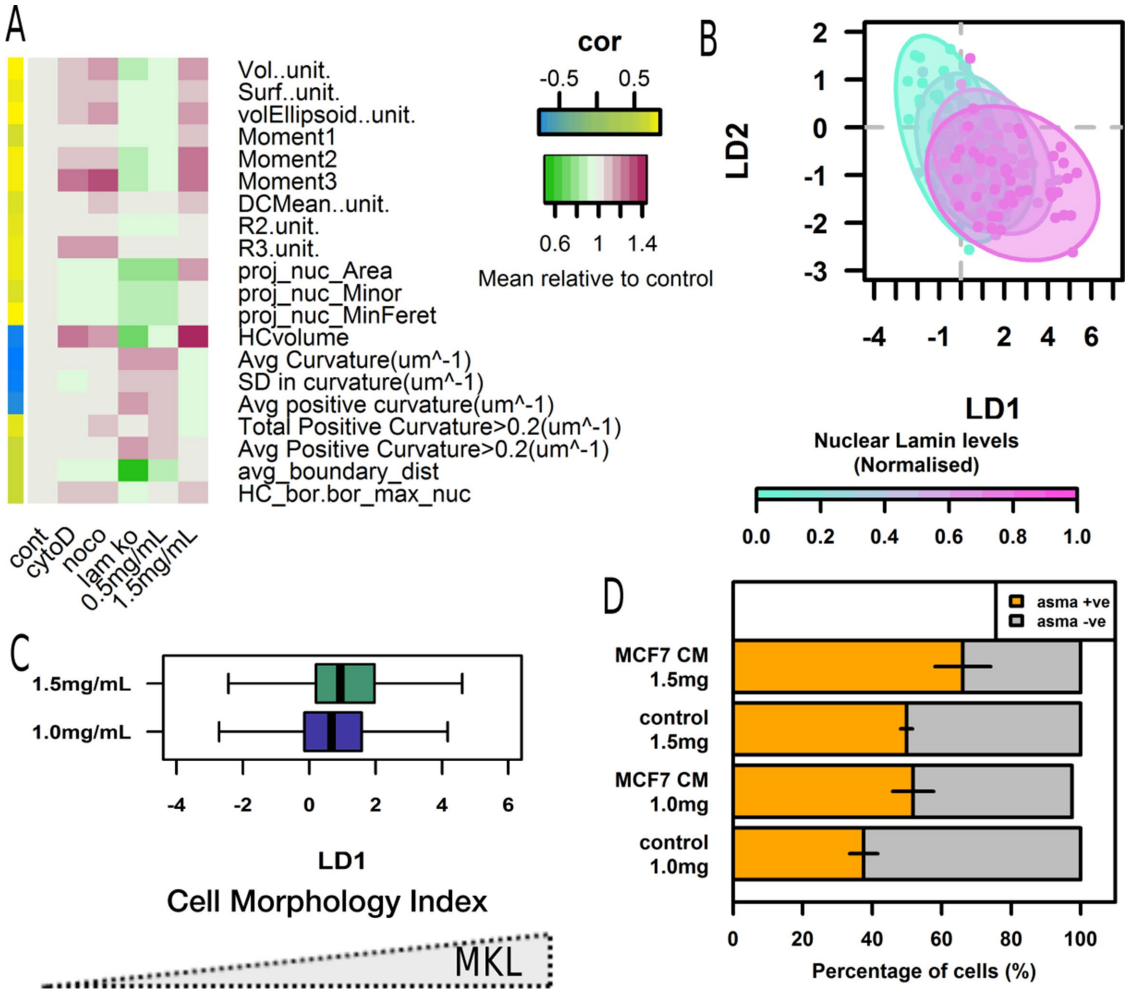

FIGURE 4: Modulating fibroblast activation by tuning the distribution cellular geometric states. (A) Heat map depicting ratio between the mean value of top parameters (depicted in Figure 3E) in a perturbed sample and control. Please note that the collagen concentration is 1 mg/ml unless otherwise state (number of fibroblasts from three trials: control, 495; nocodazole [noco], 375; cytochalasin D [cytoD], 275; 0.5 mg/ml, 425; 1.5 mg/ml, 440; Lamin A/C KO MEF [lamko], 524; MEF, 450). (B) LDA biplot of nuclear Lamin levels. Note that the loadings here is same as in Figure 3B (number of fibroblasts:110). (C) Box plot of the CMI values in NIH3T3 cells in 1.0 mg/ml and 1.5 mg/ml collagen. The means are significantly different ($p < 2.6e\text{-}6$, Wilcox's *t* test). (D) The percentage of a-SMA expressing (+ve: positive: orange) cells in the samples visualized as a stacked barplot. Segments represent the standard error of mean across three trials (number of fibroblasts: 1.0 mg/ml control: 153 and CM: 148; 1.5 mg/ml control: 130 and CM: 169). The means are significantly different ($p < 1.6e\text{-}4$, Wilcox's *t* test). CM stands for conditioned media (number of cells in each sample ~300).

distribution of geometric states should lead to altered fibroblast activation levels. Matrix rigidity, cytoskeletal filaments such as actin and microtubules, as well as the nuclear envelope proteins such as Lamin A/C have been shown to alter cell and nuclear morphology (Omelchenko *et al.*, 2002; Li *et al.*, 2014; Cho *et al.*, 2017; Kim *et al.*, 2017). Therefore, we first characterized the effects of these factors in regulating the distribution of cell geometric states in our 3D system. To measure the contribution of the actin and microtubules on cell geometric states in our system, we treated fibroblasts embedded in a collagen matrix for 24 h, with cytochalasin D (2.5 μM) and nocodazole (5 μg/ml) for 1 h. We probed the importance of Lamin A/C by using a mouse embryonic fibroblast in which Lamin A/C has been knocked out compared with the wild type control. We tested the effect of matrix rigidity by embedding fibroblasts in collagen matrix of varying concentrations (0.5, 1.0, and 1.5 mg/ml) for 24 h. We point out that in addition to increasing the stiffness of the matrix, increasing collagen concentration also alters the ligand density and fibrillar structure of the matrix.

The fold change in the mean value of parameter in the perturbed and control fibroblasts is visualized in Supplemental Figure S4A and the top 20 parameters from Figure 3E are highlighted in Figure 4A. To quantify the overall change induced by the aforementioned treatments, we computed the mean difference in the value of all parameters with respect to the control. All perturbations led to changes in different nuclear and chromatin features.

Lamin A/C depletion and increased matrix rigidity was found to cause maximal but contrasting changes to the cell geometric parameters (Supplemental Figure S4, A and B). In contrast to increased matrix rigidity, in Lamin A/C KO cells, the top parameters are associated with lower CMI (Figure 4A; Supplemental Figure S4C). For instance, as opposed to activation-primed cell geometries, LaminA/C KO cells had larger nuclei that has more curvature

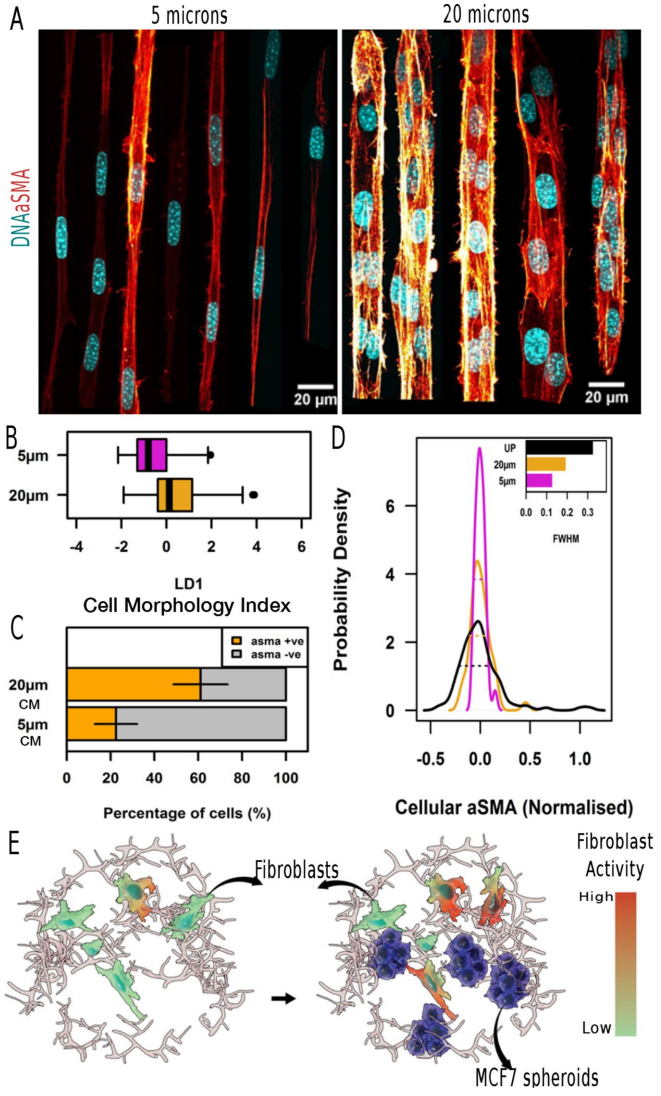

FIGURE 5: Controlling cell geometric heterogeneity allows control of fibroblast activation levels. (A) NIH3T3 cells grown on 5- and 20-μm-wide fibronectin stripes in conditioned media stained for aSMA (heat colors) and DNA (cyan) (scale bar is 20 μm). Note: This is a collage of cells from different fields of view. (B) Box plot depicting the LD1 values of cells on 5- and 20-μm-wide stripes. The means are significantly different ($p < 2.6e\text{-}6$, Wilcox's *t* test). (C) The percentage of a-SMA expressing (+ve: positive, orange) cells in the samples visualized as a stacked barplot. The means are significantly different ($p < 2.6e\text{-}6$, Wilcox's *t* test). Segments represent the standard error of mean across three trials. CM stands for conditioned media. (D) Probability density of mean centered cellular aSMA levels in unpattered cells and cells on 5- and 20-μm-wide stripes. The dotted line represents the width of each distribution at its half maxima. Inset: FWHM of the distributions. (E) A summary model.

and lower HC volume. This suggests that cell geometries with lower CMI will have reduced Lamin A/C levels. To test this, we stained fibroblasts with Lamin A/C and mapped its levels to the cell geometric state using the previously estimated PCA-LDA loadings (Figure 4B; Supplemental Figure S4, D–F). Indeed, we find that the cells with higher CMI had higher Lamin A/C levels. In contrast, the fraction of the primed cell geometric states (CMI > 0) is increased in cells embedded in 1.5 mg/ml collagen (stiff) matrix (Figure 4C). This would indicate that there would be higher levels of activation in such a stiff matrix. We next validated this by culturing fibroblasts in 1 and 1.5 mg/ml collagen in the presence and absence of conditioned media from MCF7 cells and measuring the fraction of αSMA-positive cells (Supplemental Figure S4, G and H). We find that in the control condition, the fraction of activated fibroblasts is higher in stiffer gels and this difference is further enhanced with conditioned media (Figure 4D). Collectively, these results indicate that by tuning the distribution of cell geometric states, fibroblast activation levels can be modulated.

Controlling cell geometric heterogeneity allows control of fibroblast activation levels

We next asked whether we could control the variability and levels of fibroblast activation by decomposing the distribution of geometric states into two relatively homogeneous subpopulations with distinct cell geometries. Since this can be achieved with better precision in a 2D cell culture system, we used NIH3T3 cells grown on micropatterned substrates. First, we validated that the coupling between cell geometric states and fibroblast activation is maintained in fibroblasts cultured on glass and exposed to conditioned media (Supplemental Figure S5; Supplemental Information). Next, we obtained two cell geometric populations by culturing fibroblasts on micropatterned lines that are 5 and 20 μm wide in MCF7 conditioned media. From Supplemental Figure S3F, it is evident that primed cell geometries have larger nuclei that are less elongated. Since both these features have been shown to be regulated by cell area and aspect ratio, we decided to use micropattered lines with widths of 5 and 20 μm (Figure 5A). The 5-μm-wide lines produced cells with lower CMI (Figure 5B). Therefore, we expected that the activation levels of fibroblasts to be higher when cultured on 20-μm-wide lines. Fibroblasts cultured on both lines for 72 h in the presence of conditioned media were stained for αSMA as shown in Figure 5A. As expected, the fraction of αSMA-positive cells was found to be higher in fibroblasts grown on 20-μm-wide lines (Figure 5C). Further, the variability as measured by the full width half maxima (FWHM) of the mean centered cellular αSMA levels was higher in unpattered cells relative to cells grown on 20- and 5-μm-wide lines (Figure 5D, inset). This indicates that by controlling cell geometry, one can control the variability in fibroblast activation levels. Collectively, our results reveal that the cellular geometric state is an important intrinsic cellular property that tunes fibroblast activation.

DISCUSSION

In this study, we present a framework for studying single cell heterogeneity and our results reveal the role of cell geometry in the selective activation of fibroblasts in tumor microenvironment, particularly in physiologically relevant engineered 3D tissues. In tissues, cells integrate biophysical and biochemical stimuli from their microenvironment in order to have a robust cellular response and to maintain homeostasis. Fibroblasts in the tumor-stomal environment are activated by signals such as TGFβ from the cancer cells (Lewis *et al.*, 2004; Stuelten, 2005); however, this activation is not uniform and only a subset of the fibroblast is activated. There has been a growing interest in the field in quantifying and characterizing the implications of such nongenetic heterogeneity in cellular populations (Huang, 2009; Altschuler and Wu, 2010; Komin and Skupin, 2017; Lawson *et al.*, 2018; Wang *et al.*, 2019). In this study, we hypothesized that the heterogeneity in fibroblast activation is coupled to the innate heterogeneity in the cell geometric states. To study this, we cocultured fibroblasts with MCF-7 spheroids in 3D collagen matrix, thereby mimicking a tumor microenvironment. Our

coculture platform using micropattered substrates also provides a more robust method to obtain multiple cell spheroids for generating engineered 3D tissues. As expected, we found that the nuclear abundance of MKL and the corresponding αSMA levels increase in fibroblasts in the presence of cancer cells.

To understand the role of observed geometric heterogeneity in regulating fibroblast activation, a method that allows for computing geometry dependent parameters, as well as quantifying functional content in order to compare the two at a single cell resolution, for a population of cells is required. Here we have computed multiple features that describe nuclear morphology and internal chromatin structure that delineate cell geometric states in a heterogeneous cell population. Recent studies have used multilinear regression models to show the importance of cell shape in YAP and NFkB (p65) signaling (Sero *et al.*, 2015; Sero and Bakal, 2017). In this study, we discretized the population-based nuclear MKL levels and demonstrated the discriminatory potential of the reduced cell geometric feature space in the classification of the identified subpopulations in both control and cocultured fibroblasts. Further, we show that the cell geometric states are correlated to nuclear MKL abundance and describe this using a linear regression model. Importantly, our observations indicate the presence of certain primed cell geometries (CMI > 0; Figure 3C) that present higher activation levels which are further enhanced in the presence of stimuli from cancer cells.

These primed cells have larger nuclei that have smoother boundaries with centrally positioned and spatially separated HC nodes. The nuclear morphology is an important regulator of the organization of chromatin within and thereby their transcriptome. While transcriptional implications of the organization of HC nodes cannot be directly deduced without knowing the identity of the genes that are packed in these regions, a change in their positioning is an indication of large scale reorganizations in the 3D chromatin organization, which is a critical modulator of transcription (Belyaeva *et al.*, 2017). Nuclear mechanical properties are dictated by Lamin A/C and its lower levels have been associated with softer nuclei that are more prone to deformations that arise due to the active state of the cytoplasm (Makhija *et al.*, 2015; Kim *et al.*, 2017). Consistently, we find that the Lamin A/C levels are correlated with cell geometric states as defined by CMI, where the activation primed cell geometric states present higher Lamin A/C levels. By increasing the matrix rigidity, we observed a shift in the distribution of cell geometric states toward higher CMI (more primed cells). As expected, the cells in stiffer gels had higher activation levels which became more pronounced in the presence of signals from cancer cells. To further prove a causal relationship between cell geometry and fibroblast activation, we cultured fibroblasts on fibronectin coated lines of 5 and 20 μm width in the cancer cell-conditioned media. Fibroblast cells on 20 μm width were enriched for primed cell geometric states (higher CMI) and these cells presented higher levels of activation.

Collectively, our results highlight the presence of activation-primed cell geometric states. In a heterogeneous tissue microenvironment, there are multiple subpopulations of fibroblasts characterized by their differential molecular, transcriptional, and morphological properties (Bauer *et al.*, 2010; Kiskowski *et al.*, 2011; Öhlund *et al.*, 2014; Avery *et al.*, 2018; Nassiri and McCall, 2018; Philippeos *et al.*, 2018; Xie *et al.*, 2018). Hence, we posit that the fibroblasts with such primed geometries in the presence of cancer cells form a subpopulation of cells that are selectively activated. In tissues, this subpopulation of active cells plays an important role in the progression of many diseases including cancers and as a result, there is a growing interest in using them as therapeutic targets (Li *et al.*, 2016; Hanley *et al.*, 2018). In diseased conditions, such intrinsic heterogeneity has been a major source of impediment for interventions that target cancer-associated fibroblasts. Our findings suggest that targeted inhibition of the activation-primed cell geometric states could pave the way for developing drug discovery pipelines for tumor models.

MATERIALS AND METHODS

Cell culture, conditioned media preparation, and treatments

NIH3T3 fibroblast and MCF7 metastatic breast cancer cells were cultured in high glucose DMEM (Life Technologies) supplemented with 10% (vol/vol) fetal bovine serum (GIBCO, Life Technologies) and 1% Penn Strep at 37°C in 5% CO_2. Conditioned media from MCF7 cells were obtained by washing and adding fresh culture media to a 70% confluent culture and collecting the media after 24 h, filtering it through a 0.2-mm syringe filter, and storing aliquots at –80°C. Cells were treated with MCF7-conditioned media for 3 d or 2.5 μM Cytochalasin-D (Sigma-Aldrich) and 5 μg/ml nocodazole (Sigma-Aldrich) for 1 h followed by fixation with 4% paraformaldehyde (Sigma) in 1× phosphate-buffered saline (PBS).

Micropatterning

Polydimethylsiloxane (PDMS) stamps were prepared by mixing PDMS elastomer (SYLGARD 184; Dow Corning) with curative-to-precursor in a 1:10 ratio according to the manufacturer's protocol and by molding the PDMS in microfabricated silicon wafers. Fibronectin solution (100 μg/ml) was then allowed to adsorb onto the surface of each PDMS stamp under sterile conditions. The coated PDMS stamp was subsequently deposited onto the surface of a nontreated hydrophobic dish (Ibidi) to allow the microfeatures to be transferred. The surface was then treated with 2 mg/ml Pluronic F-127 (Sigma-Aldrich) for 30 min to passivate nonfibronectin-coated regions. Thirty thousand cells were seeded for 15 min. Unadhered cells were removed, and the remaining cells were washed once with 1× PBS and 1 ml of cell culture media and incubated for 3 h.

3D coculture

To generate spheroids, MCF7 cells (1×10^6) were seeded on fibronectin-coated circular micropatterns of area 1800 μm^2. After 24 h, the MCF7 cells formed clumps with 7–10 cells/clump. These clumps were scrapped and mixed with 50,000 NIH3T3 cells trypsinized from a 70% confluent culture in a 1 mg/ml rat tail collagen I (ThermoFisher Scientific) solution which was neutralized with 0.1 N NaOH. In control samples, only NIH3T3 cells were used. This solution was allowed to gel at 37°C for 3 h after which 0.5 ml of culture media was added and the samples were kept for 24–72 h.

Immunostaining 3D culture samples

Gels were rinsed twice with 1× PBS, followed by fixation using 4% paraformaldehyde (Sigma) for 20 min. Cells were washed and permeabilized with 0.2% Triton-X (Sigma) in 1× PBS for 30 min. After washing thrice with 1× PBS, the cells were treated with 5% bovine serum albumin (BSA) (blocking solution) for 3 h. This was followed by incubation with required primary antibodies (in blocking buffer) overnight at 4°C. The primary antibodies were myocardin-related transcription factor (MRTF-A) (1:200; Santa Cruz; and 1:500 AbCAM), and αSMA (1:250; Cell Signaling). Cells were washed thrice for 15 min with washing solution (0.1% triton and 0.1% Tween) and incubated with corresponding Alexa Fluor secondary antibody along with Hoescht-33342 (1 mg/ml; 1:1000) for 3 h. Filamentous actin (F-actin) was labeled using phalloidin Alexa Fluor 488 (1:1000;

Life Technologies). The samples were washed with washing solution thrice for 15 min and imaged.

Immunostaining 2D culture samples

Cells were rinsed twice with 1× PBS, followed by fixation using 4% paraformaldehyde (Sigma) for 20 min. Cells were washed and permeabilized with 0.2% Triton-X (Sigma) in 1× PBS for 15 min. After being washed twice with 1× PBS, the cells were treated with 5% BSA (blocking solution) for 1 h. This was followed by incubation with required primary antibodies (in blocking buffer) overnight at 4°C. The primary antibodies were MRTF-A/MKL (1:400; Santa Cruz and 1:800 AbCAM) and αSMA (1:450 Cell Signaling). Cells were washed with blocking solution and incubated with corresponding Alexa Fluor secondary antibody along with Hoescht-33342 (1 mg/ml; 1:1000) for 45 min. F-actin was labeled using phalloidin Alexa Fluor 488 (1:1000; Life Technologies). The samples were washed and imaged.

Confocal imaging and image analysis

The 2D culture samples were scanned using Nikon A1 Confocal microscope (Nikon, USA) with a 100× 1.4 NA oil immersion objective. Stacks of 16-bit gray scale 2D images were obtained with a voxel size of 120 nm in the XY direction and 500 nm in the Z direction. The 3D culture samples were scanned with a 60× 1.25 NA oil immersion objective. Stacks of 16-bit gray scale 2D images were obtained with a voxel size of 120 nm in the XY direction and 800 nm in the Z direction.

Images were analyzed using custom codes written in ImageJ2/Fiji (Schindelin *et al.*, 2012) and MATLAB using the functions from Bioformats, mcib3d, and Image Processing Library (Toolbox, 2004). The raw 3D images labeled for DNA were processed using a Gaussian blur filter (Sigma 0.15) and thresholded using Otsu, a global thresholding method, to binarize and identify the nuclear regions. Watershed was then used to separate touching nuclei. This binary image was then used to identify individual nuclei as 3D objects within a size range of 200–1300 μm^3, and this was followed by cropping of individual nuclei in all four channels along their bounding rectangles. These individual nuclear crops were used to quantify 3D nuclear parameters and the respective maximum intensity projections were used to measure 2D parameters.

HC nodes were identified from DNA intensity images based on an intensity and volume threshold: pixels with intensity more than $\text{Lowerthreshold}_{HC}$ were first binarized and 3D nodes were identified as those objects with volumes of at least 1 μm^3:

$$\text{Lowerthreshold}_{HC} = \text{Mean}_{DNA} + 1.5 \times (\text{StandardDeviation}_{DNA})$$

The nuclear intensity and compaction features were identified from the DNA intensity images and from the HC regions identified as described above. The population descriptors (mean, median, max, min, and SD) of the geometric and the positioning parameters of the HC nodes were then calculated for each individual nucleus. The complete feature list can be found in the Supplemental Information.

The MKL nuclear levels and cellular αSMA from each experiment were normalized by setting the maximum intensity value to 1 in order to compare across trials.

The cellular αSMA levels are represented by the mean levels of αSMA in a perinuclear ring of 2 µm width in 3D. The αSMA-positive cells were identified using a threshold, defined as the median levels of cellular αSMA in both control, and cocultured fibroblasts/fibroblasts in conditioned media.

Statistical analysis

All statistical analyses and plotting were carried out in R (R Development Core Team, 2016). For each parameter set, feature reduction by PCA using correlation matrix obtained from the scaled data was used. The scores from the first three principle components were then used as discriminant variables in LDA (library MASS) to separate the different classes. The first or the first two LDs along with 95% confidence ellipsoids (libraries sp, rgeos) were used to visualize the separation between the classes. To calculate the degree of separation, the intersection ratio as defined below is used. In cases where there are more than one class, a matrix consisting of the pairwise intersection ratio of the various classes is computed and visualized as a heat map:

$$\text{IntersectionRatio} = \frac{\text{IntersectionArea}}{\left(\text{Area}_{\text{ellipsoid1}} + \text{Area}_{\text{ellipsoid2}}\right)}$$

Continuous variables such as the nuclear intensity of transcription factors have been binned to generate 10 equal subpopulations based on the population deciles. In such cases, a plot of mean intersection ratio as a function of number of deciles apart of the different parameter sets is also computed to depict the degree of separation as a function of the increasing nuclear intensity. Linear regression models employing nuclear transcription factor levels as a function of the LD1 have been used.

ACKNOWLEDGMENTS

We thank Caroline Uhler for helpful discussions. In addition, we thank Danai Kati for help with some of the experiments and Diego Pitta de Araujo for preparing the illustrations. Lamin A/C knockdown MEFs were kind gifts from the Colin Stewart Laboratories. We thank the MechanoBiology Institute, National University of Singapore, Ministry of Education Tier-3 program (2012-T3-1-001) and the Institute of Molecular Oncology, Italian Foundation for Cancer Research and Mechanobiology Institute Joint-Research Laboratory for funding.

REFERENCES

Altschuler SJ, Wu LF (2010). Cellular heterogeneity: do differences make a difference? Cell 141, 559–563.

Asghar W, El Assal R, Shafiee H, Pitteri S, Paulmurugan R, Demirci U (2015). Engineering cancer microenvironments for in vitro 3-D tumor models. Mater Today 18, 539–553.

Avery D, Govindaraju P, Jacob M, Todd L, Monslow J, Puré E (2018). Extracellular matrix directs phenotypic heterogeneity of activated fibroblasts. Matrix Biol 67, 90–106.

Bauer M, Su G, Casper C, He R, Rehrauer W, Friedl A (2010). Heterogeneity of gene expression in stromal fibroblasts of human breast carcinomas and normal breast. Oncogene 29, 1732–1740.

Belyaeva A, Venkatachalapathy S, Nagarajan M, Shivashankar GV, Uhler C (2017). Network analysis identifies chromosome intermingling regions as regulatory hotspots for transcription. Proc Natl Acad Sci USA 114, 13714–13719.

Chen CS, Mrksich M, Huang S, Whitesides GM, Ingber DE (1997). Geometric control of cell life and death. Science 276, 1425–1428.

Cho S, Irianto J, Discher DE (2017). Mechanosensing by the nucleus: from pathways to scaling relationships. J Cell Biol 216, 305–315.

Damodaran K, Venkatachalapathy S, Alisafaei F, Radhakrishnan AV, Sharma Jokhun D, Shenoy VB, Shivashankar GV (2018). Compressive force induces reversible chromatin condensation and cell geometry–dependent transcriptional response. Mol Biol Cell 29, 3039–3051.

Erdogan B, Ao M, White LM, Means AL, Brewer BM, Yang L, Washington MK, Shi C, Franco OE, Weaver AM, *et al.* (2017). Cancer-associated fibroblasts promote directional cancer cell migration by aligning fibronectin. J Cell Biol 216, 3799–3816.

Grinnell F (2003). Fibroblast biology in three-dimensional collagen matrices. Trends Cell Biol 13, 264–269.

Hanley CJ, Mellone M, Ford K, Thirdborough SM, Mellows T, Frampton SJ, Smith DM, Harden E, Szyndralewiez C, Bullock M, *et al.* (2018).

Targeting the myofibroblastic cancer-associated fibroblast phenotype through inhibition of NOX4. J Natl Cancer Inst 110, 109–120.
Herum KM, Choppe J, Kumar A, Engler AJ, McCulloch AD (2017). Mechanical regulation of cardiac fibroblast profibrotic phenotypes. Mol Biol Cell.
Hinz B, Celetta G, Tomasek JJ, Gabbiani G, Chaponnier C (2013). Alpha-smooth muscle actin expression upregulates fibroblast contractile activity. Mol Biol Cell 12, 2730–2741.
Huang S (2009). Non-genetic heterogeneity of cells in development: more than just noise. Development 136, 3853–3862.
Jain AK, Duin RPW, Mao J (2000). Statistical pattern recognition: a review. IEEE Trans Pattern Anal Mach Intell 22, 4–37.
Jain N, Iyer KV, Kumar A, Shivashankar GV (2013). Cell geometric constraints induce modular gene-expression patterns via redistribution of HDAC3 regulated by actomyosin contractility. Proc Natl Acad Sci USA 110, 11349–11354.
Kalluri R (2016). The biology and function of fibroblasts in cancer. Nat Rev Cancer 16, 582.
Kim JK, Louhghalam A, Lee G, Schafer BW, Wirtz D, Kim DH (2017). Nuclear lamin A/C harnesses the perinuclear apical actin cables to protect nuclear morphology. Nat Commun 8, 1–13.
Kiskowski MA, Jackson RS, Banerjee J, Li X, Kang M, Iturregui JM, Franco OE, Hayward SW, Bhowmick NA (2011). Role for stromal heterogeneity in prostate tumorigenesis. Cancer Res 71, 3459–3470.
Komin N, Skupin A (2017). How to address cellular heterogeneity by distribution biology. Curr Opin Syst Biol 3, 154–160.
Labriola NR, Darling EM (2015). Temporal heterogeneity in single-cell gene expression and mechanical properties during adipogenic differentiation. J Biomech 48, 1058–1066.
Lawson DA, Kessenbrock K, Davis RT, Pervolarakis N, Werb Z (2018). Tumour heterogeneity and metastasis at single-cell resolution. Nat Cell Biol 20, 1349–1360.
Lee WC, Shi H, Poon Z, Nyan LM, Kaushik T, Shivashankar GV, Chan JKY, Lim CT, Han J, Van Vliet KJ (2014). Multivariate biophysical markers predictive of mesenchymal stromal cell multipotency. Proc Natl Acad Sci USA 111, E4409–E4418.
Lewis MP, Lygoe KA, Nystrom ML, Anderson WP, Speight PM, Marshall JF, Thomas GJ (2004). Tumour-derived TGF-β1 modulates myofibroblast differentiation and promotes HGF/SF-dependent invasion of squamous carcinoma cells. Br J Cancer 90, 822–832.
Li M, Li M, Yin T, Shi H, Wen Y, Zhang B, Chen M, Xu G, Ren K, Wei Y (2016). Targeting of cancer-associated fibroblasts enhances the efficacy of cancer chemotherapy by regulating the tumor microenvironment. Mol Med Rep 13, 2476–2484.
Li Q, Kumar A, Makhija E, Shivashankar GV (2014). The regulation of dynamic mechanical coupling between actin cytoskeleton and nucleus by matrix geometry. Biomaterials 35, 961–969.
Li Q, Makhija E, Hameed FM, Shivashankar GV (2015). Micropillar displacements by cell traction forces are mechanically correlated with nuclear dynamics. Biochem Biophys Res Commun 461, 372–377.
Makhija E, Jokhun DS, Shivashankar GV (2015). Nuclear deformability and telomere dynamics are regulated by cell geometric constraints. Proc Natl Acad Sci USA 113, E32–E40.
McWhorter FY, Wang T, Nguyen P, Chung T, Liu WF (2013). Modulation of macrophage phenotype by cell shape. Proc Natl Acad Sci USA 110, 17253–17258.
Miralles F, Posern G, Zaromytidou AI, Treisman R (2003). Actin dynamics control SRF activity by regulation of its coactivator MAL. Cell 113, 329–342.
Mitra A, Venkatachalapathy S, Ratna P, Wang Y, Jokhun DS, Shivashankar GV. (2017). Cell geometry dictates TNFα-induced genome response. Proc Natl Acad Sci USA 114, E3882–E3891.
Nassiri I, McCall MN (2018). Systematic exploration of cell morphological phenotypes associated with a transcriptomic query. Nucleic Acids Res 46, e116.
Öhlund D, Elyada E, Tuveson D (2014). Fibroblast heterogeneity in the cancer wound. J Exp Med 211, 1503–1523.
Omelchenko T, Vasiliev JM, Gelfand IM, Feder HH, Bonder EM (2002). Mechanisms of polarization of the shape of fibroblasts and epitheliocytes: separation of the roles of microtubules and Rho-dependent actin-myosin contractility. Proc Natl Acad Sci USA 99, 10452–11045.
Philippeos C, Telerman SB, Oulès B, Pisco AO, Shaw TJ, Elgueta R, Lombardi G, Driskell RR, Soldin M, Lynch MD, *et al*. (2018). Spatial and single-cell transcriptional profiling identifies functionally distinct human dermal fibroblast subpopulations. J Invest Dermatol 138, 811–825.
R Development Core Team (2016). R: a language and environment for statistical computing. R Found Stat Comput, www.R-project.org.
Richards KE, Zeleniak AE, Fishel ML, Wu J, Littlepage LE, Hill R (2017). Cancer-associated fibroblast exosomes regulate survival and proliferation of pancreatic cancer cells. Oncogene 36, 1770–1778.
Roy B, Venkatachalapathy S, Ratna P, Wang Y, Jokhun DS, Nagarajan M, Shivashankar GV (2018). Laterally confined growth of cells induces nuclear reprogramming in the absence of exogenous biochemical factors. Proc Natl Acad Sci USA 115, E4741–E4750.
Schindelin J, Arganda-Carreras I, Frise E, Kaynig V, Longair M, Pietzsch T, Preibisch S, Rueden C, Saalfeld S, Schmid B, *et al*. (2012). Fiji: an open-source platform for biological-image analysis. Nat Methods 9, 676–682.
Sero JE, Bakal C (2017). Multiparametric analysis of cell shape demonstrates that β-PIX directly couples yap activation to extracellular matrix adhesion. Cell Syst 4, 84–96.
Sero JE, Sailem HZ, Ardy RC, Almuttaqi H, Zhang T, Bakal C (2015). Cell shape and the microenvironment regulate nuclear translocation of NF- κB in breast epithelial and tumor cells. Mol Syst Biol 11, 790.
Stuelten CH (2005). Breast cancer cells induce stromal fibroblasts to express MMP-9 via secretion of TNF- and TGF-. J Cell Sci 118, 2143–2153.
Théry M (2003). Micropatterning as a tool to decipher cell morphogenesis and functions. J Cell Sci 123, 4201–4213.
Toolbox IP (2004). Image processing toolbox, MATLAB.
Tsuboi A, Umetsu D, Kuranaga E, Fujimoto K (2017). Inference of cell mechanics in heterogeneous epithelial tissue based on multivariate clone shape quantification. Front Cell Dev Biol 5, 68.
Uhler C, Shivashankar GV (2017). Regulation of genome organization and gene expression by nuclear mechanotransduction. Nat Rev Mol Cell Biol 18, 717–727.
Wang N, Zheng J, Chen Z, Liu Y, Dura B, Kwak M, Xavier-Ferrucio J, Lu YC, Zhang M, Roden C, *et al*. (2019). Single-cell microRNA-mRNA co-sequencing reveals non-genetic heterogeneity and mechanisms of microRNA regulation. Nat Commun 10, 1–12.
Wang Y, Nagarajan M, Uhler C, Shivashankar GV (2017). Orientation and repositioning of chromosomes correlate with cell geometry–dependent gene expression. Mol Biol Cell 28, 1997–2009.
Xie T, Wang Y, Deng N, Huang G, Taghavifar F, Geng Y, Liu N, Kulur V, Yao C, Chen P, *et al*. (2018). Single-cell deconvolution of fibroblast heterogeneity in mouse pulmonary fibrosis. Cell Rep 22, 3625–3640.
Yang TH, Thoreson AR, Gingery A, An KN, Larson DR, Zhao C, Amadio PC (2015). Collagen gel contraction as a measure of fibroblast function in carpal tunnel syndrome. J Biomed Mater Res Part A 103, 574–580.